Indian J Phys
https://doi.org/10.1007/s12648-024-03428-5

ORIGINAL PAPER

Nuanced synthesis strategies and comprehensive analysis of intricate multifarious luminescent phosphor hosts

R Kiran[1], N S Prabhu[2], V Mishra[1], M I Sayyed[3,4] and S D Kamath[1]*

[1]Department of Physics, Manipal Institute of Technology, Manipal Academy of Higher Education, Manipal, Karnataka, India

[2]Department of Physics, Indian Institute of Science, Bangalore 560012, India

[3]Department of Physics, Faculty of Science, Isra University, Amman, Jordan

[4]Department of Physics and Technical Sciences, Western Caspian University, Baku, Azerbaijan

Received: 23 January 2024 / Accepted: 13 September 2024

Abstract: This paper primarily addresses various methodologies for synthesizing novel phosphors, with our focus mainly on the mixed alkaline tungstate phosphor Ca_2MgWO_6. In the initial synthesis phase, we used precisely weighed $CaCO_3$, MgO, and WO_3 for the synthesis. The XRD patterns indicated the presence of an impure phase, specifically $CaWO_4$, in the resulting product. We adeptly tackled the formation of $CaWO_4$ and mitigated it by employing a multifaceted approach. These included adding an excess amount of MgO, opting for an alternative chemical route, and the incorporation of flux during synthesis. It was observed that the product obtained through the addition of flux exhibited a purity level of approximately 99.75% with a margin of error of ± 0.02%. Ultimately, we have carried out structural, morphological, optical, and thermal characterizations, along with density functional theory (DFT) simulations, to assess the fundamental parameters of the pure sample.

Keywords: Phosphors; X-ray techniques; Spectroscopy; Thermal analysis; DFT

Introduction

Phosphors or luminescent materials are a domain of significant fascination in modern science due to their vast applications in day-to-day life. Hence, a considerable amount of work is going on various phosphor hosts which include oxides, vanadates, silicates, tungstates, niobates, etc [1, 2]. However, in most of the works we have come across, the XRD patterns of the phosphors showed the presence of impure phases which in turn might affect their overall performance [3, 4]. Hence to overcome this predicament, we have handpicked Ca_2MgWO_6 (CMW) as our phosphor host and illustrated various experimental courses one can opt to produce the purer CMW phosphor by lowering the presence of impure phase. We have also illustrated the approach one should adopt to systematically analyze their characteristics. CMW belongs to the family of mixed alkaline earth tungstate phosphors, characterized by the overarching chemical formula A_2BWO_6 (A = Ca, Sr, and Ba; B = Mg, Ni, Fe, Co, and Zn) with a double perovskite structural arrangement [5]. Its crystal structure is essentially governed by the ionic radii and charges of the A, B, and W^{6+} cations, showcasing their intricate and sophisticated crystalline composition [6]. Depending on various physical conditions, the cation arrangements will change and result in cubic, tetragonal, and orthorhombic crystal structures [7]. To date, many phosphors have been reported with Ca_2MgWO_6 as a phosphor host. To name a few Ca_2MgWO_6: Bi^{3+}, Ca_2MgWO_6:Cr^{3+}, Ca_2MgWO_6:Sm^{3+}/Bi^{3+}, Ca_2MgWO_6:Cr^{3+}/Nd^{3+} and Ca_2MgWO_6: Cr^{3+}/Yb^{3+} [8–12]. But in most of the works, the impurity phase was observed and the method of elimination of impurities is not mentioned. In several studies, various strategies have been proposed to mitigate the formation of impurities in compounds. For instance, in the case of $A_2Mg_{2-2x}Dy_xLi_xWO_6$ (A = Ca, Sr, Ba) [13], Ba_2MgWO_6: Eu^{3+} [14], Ba_2MgWO_6: Er^{3+} [15], Ba_2MgWO_6: Nd^{3+} [16], Sr_2MgWO_6:Ni^{2+} [17], Ba_2MgWO_6:Dy^{3+} and Ba_2MgWO_6:Sm^{3+}, excess amount of magnesium compound is added [18, 19]. In the case of

*Corresponding author, E-mail: sudhakamath6@gmail.com

Published online: 07 October 2024

$Ca_2MgWO_6:Bi^{3+}$, MgF_2 was used as a flux to eliminate the impure phase [20].

Therefore, in the present work, we have taken a few approaches to synthesize the pure CMW phosphor host. The experimental measures for the production of purer samples mainly involve modifying the synthesis process and changing the conditions used during the high-temperature solid-state reaction method.

In the initial approach, we added an excess amount of MgO to overcome the occurrence of stoichiometric imbalance in the chemical mixture at high temperatures [21]. In the succeeding approach, an alternate chemical i.e. CaO was used as a precursor instead of $CaCO_3$ since CaO is more thermally stable as compared to $CaCO_3$ [22]. Finally, we added various concentrations of MgF_2 as the flux along with the raw chemicals during the synthesis process and studied the effects of MgF_2 concentrations on the amount of $CaWO_4$ in the sample [23]. Furthermore, the results of each approach are evaluated to put forward the optimum synthesis method to produce the best quality CMW phosphor. After the synthesis of the host, we carry out various characterizations and DFT simulations to study the structural, optical, morphological, and thermal properties of the phosphor.

Experimental details

Material synthesis

Ca_2MgWO_6 was prepared via a high-temperature solid-state reaction method using stoichiometric amounts of $CaCO_3$, MgO, and WO_3. The mixture was ground for 1 hour using mortar and pestle, transferred to an alumina crucible, and heated for 5 h at 600 °C in a muffle furnace. After cooling the mixture to room temperature, it was ground again for 1 hour and heated for 5 h at 1200 °C as shown in Fig. 1(a). To minimize the formation of impure phase $CaWO_4$, additional batches were prepared with variations: CaO was used instead of $CaCO_3$ as the starting chemical, excess MgO (10, 15, 20, and 200 wt%) was added with initial precursors, and $xMgF_2$ (x = 1.5, 1.75, 2 and 3 wt%) was used as flux with initial chemicals. Extra MgF_2 remaining in the CMW sample was eliminated by dissolving it in conc.HNO_3, followed by filtration and heating at 600 °C as shown in Fig. 1(b).

Characterization techniques

The crystal structure was evaluated using powder XRD using Rigaku Miniflex 600 (5th gen) with K_α radiation ($\lambda = 1.54059$ nm). Additionally, Fourier Transformed Infrared Spectroscopy (FTIR) was also employed in the analysis. Morphological investigations were conducted through the utilization of a Scanning Electron Microscope (SEM). The exploration of optical characteristics encompassed a meticulous examination of emission and excitation spectra, which was accomplished through the acquisition of data via the JASCO FP-800 spectrofluorometer. The diffused reflectance spectra of the phosphor were acquired employing the Perkin Elmer Lambda 900 spectrophotometer. Subsequently, a rigorous investigation of the thermal properties was carried out by utilizing a Thermo Gravimetric Analyzer. Quantum Espresso code was used to simulate the density of states and optical absorption spectra of the Ca_2MgWO_6 using a density functional theory [24]. The self-consistent computations achieve convergence when the total energy of the system remains constant within a range of 1×10^{-3} mRy. The relaxation of the structure takes place after the energy convergence reaches 6×10^{-5} eV and continues until the forces per atom reduce to 0.05 eV [25].

Results and discussions

Synthesis of pure CMW phosphor

To begin with, we synthesize CMW phosphor through a solid-state reaction method using $CaCO_3$, MgO, and WO_3. The XRD patterns of the product is shown in Fig. 2 and it is unmistakably clear that the pattern has a striking resemblance to the reference pattern of CMW (JCPDS# 48-0108) signifying the successful synthesis of the desired compound. However, it is also noticeable that the XRD pattern contains additional peaks corresponding to the impure phase $CaWO_4$ (JCPDS# 41-1413). The existence of $CaWO_4$ raises concerns, as it may influence the properties and performance of the CMW phosphor. Hence it is necessary to further investigate and improve the synthesis process to enhance the purity of the phosphor.

To investigate the root cause of impurity formation, we conducted Thermogravimetric Analysis (TGA) on raw chemicals at a heating rate of 5 °C/min [26]. We additionally include CaO in the TGA study because $CaCO_3$ rapidly decomposes to CaO with the emission of CO_2 beyond 750 °C. Figure 3(a) shows the outcome of TGA studies and it becomes apparent that the formation of impurities can be attributed to the reduction in MgO mass during the heating process. The diminishment of the MgO mass disrupts the stoichiometric ratios of the raw chemicals, leading to a situation where $CaCO_3$ and WO_3 can react with each other, ultimately resulting in the formation of $CaWO_4$. Therefore, to get the purer compound, we implement the following modifications to the synthesis

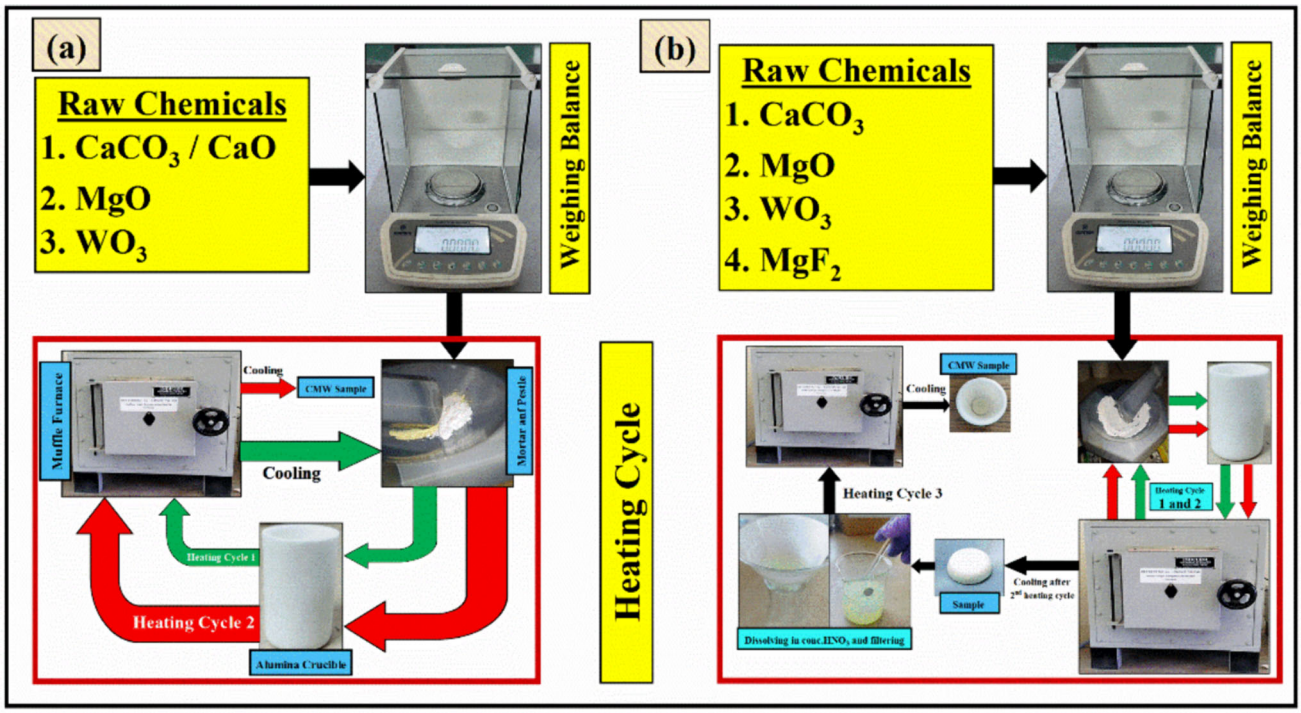

Fig. 1 (a)–(b) Synthesis routes of CMW phosphor

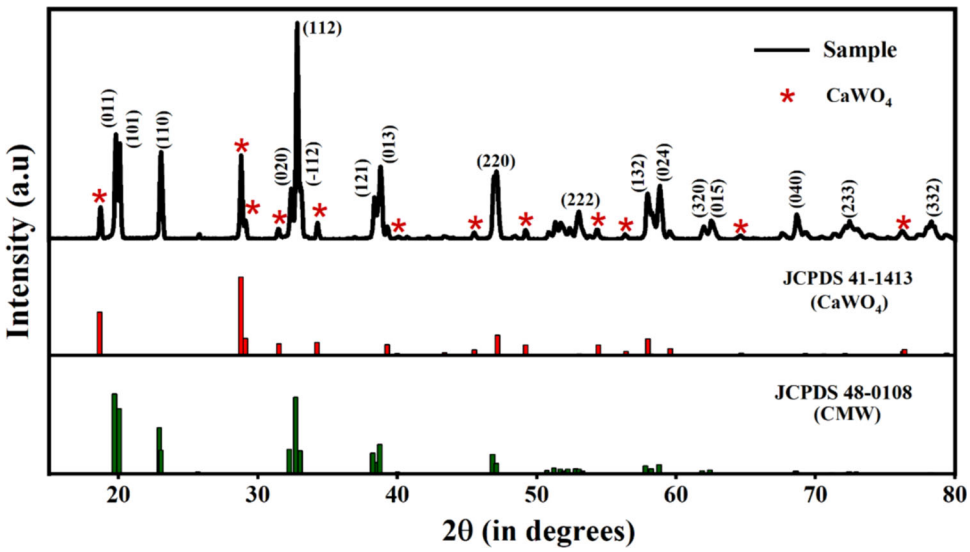

Fig. 2 XRD patterns of JCPDS card no. 48–0108 (CMW), 41–1413 ($CaWO_4$), and prepared CMW phosphor sample

process to minimize the formation of $CaWO_4$ as much as possible.

Using CaO as a precursor instead of $CaCO_3$

A noteworthy observation from Fig. 3(a) indicates that CaO demonstrates greater thermal stability of CaO when juxtaposed with $CaCO_3$. As a consequence, CaO can serve as a more appropriate precursor in place of $CaCO_3$. We adhere to the same synthesis procedure to obtain the sample and to confirm the formation of the product, XRD analysis is conducted. The XRD patterns of the phosphor are given in Fig. 3(b) and it is noticeable that in comparison to Fig. 2, there is a slight increase in the intensity of impurity peaks. The reason for this observation is that both WO_3 and CaO are thermally stable and due to this, the reaction between them will be more efficient. This results in excess $CaWO_4$ formation, which in turn causes the impurity peaks to become more pronounced. Therefore, we can discard this method for the synthesis of phosphor.

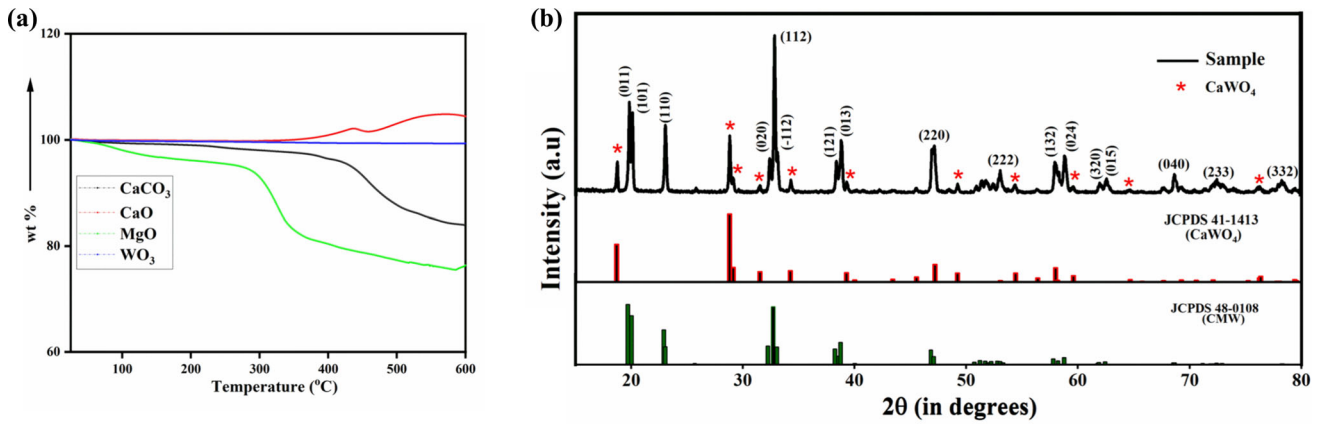

Fig. 3 (a) TGA curve of precursors and (b) XRD patterns of JCPDS card no. 48–0108 (CMW), 41–1413 ($CaWO_4$), and blank CMW with CaO as the precursor

Adding an excessive amount of MgO One of the commonly advocated methodologies to reduce $CaWO_4$ is by incorporating excess MgO during the synthesis, aimed at compensating for the potential loss of MgO mass. Fig. 4(a) displays the XRD pattern of the prepared sample with varying amounts of excess MgO (10%, 15%, 20%, and 200%) during the initial mixing stage. As we increased the excess of MgO from 10 to 200%, a discernible reduction in the intensity of the impurity peak was indeed observed. Nevertheless, it is worth noting that the magnitude of MgO required to elicit visible alterations in the XRD patterns was quite substantial. Therefore, we can conclude that this particular method does not represent the optimal approach for synthesizing pure CMW, as the effectiveness of impurity reduction is not commensurate with the significant quantities of MgO demanded to achieve these marginal improvements.

Using MgF_2 as a flux Finally, we tried out a new approach in which we utilized MgF_2 as flux because it oxidizes to MgO on heating [27]. We incorporated various amounts of MgF_2 (1.5, 1.75, 2, and 3 wt%) along with the stoichiometric amount of starting materials $CaCO_3$, MgO, and WO_3. The XRD patterns of the sample are given in Fig. 4(b), and it can be seen that the intensity of impure peaks decreases as we increase the amount of MgF_2 from 1.5 to 3 wt%. We have stopped the addition of MgF_2 at 3 wt% because further addition will result in an increase in MgF_2 signature peaks in the XRD patterns.

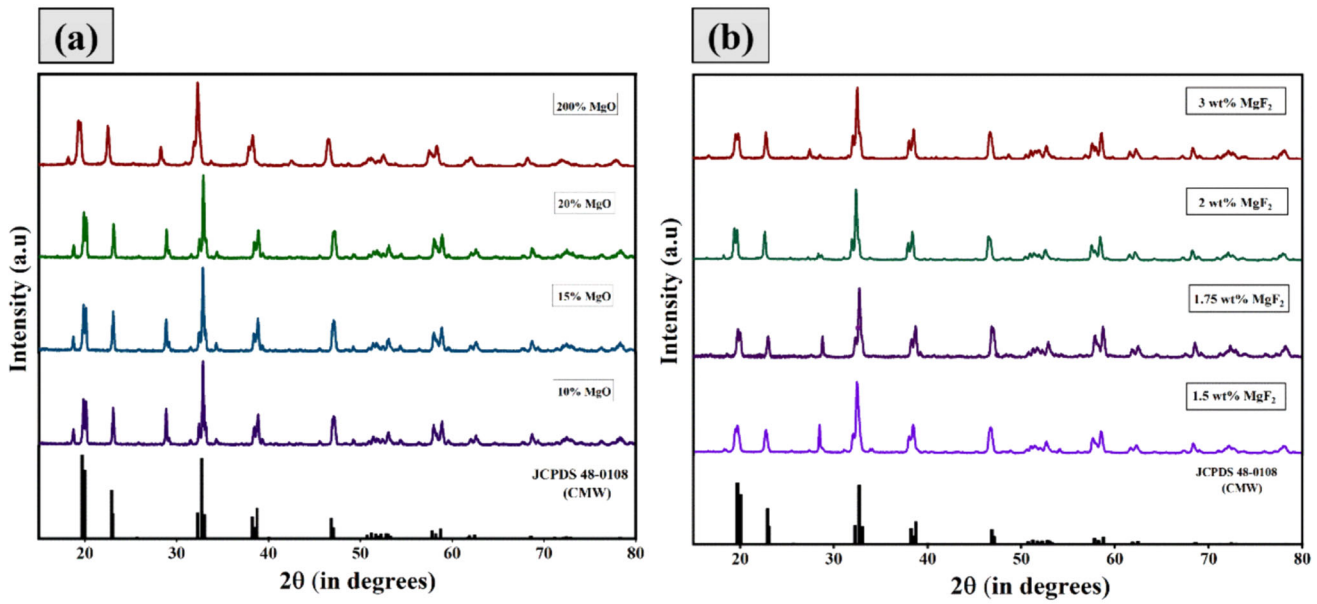

Fig. 4 XRD patterns of prepared CMW phosphor with (a) 10%, 15%, 20%, and 200% extra MgO as the precursor (b) 1.5%, 1.75%, 2% and 3% MgF_2 as flux

We also noticed the presence of additional peaks that correspond to non-oxidized MgF_2. To eliminate the non-oxidized MgF_2 present in the sample, the sample is dissolved in a solvent mixture of conc.HNO_3. Once dissolved, we filtered the solution using Whatman filter paper and subsequently subjected it to a heat treatment at 600 °C for a duration of 2 h to eliminate any residual solvent components. Following this treatment, we conducted an XRD analysis of the sample, the results of which are presented in Fig. 5(a). It is evident from figure that previously observed extra peaks are no longer present. This indicates that the CMW phosphor is successfully synthesized and is used for further studies using different characterization techniques.

Evaluation of fundamental parameters of CMW

We commence our evaluation process by refining the XRD data using FullProf software considering both CWM and $CaWO_4$ phases to ascertain the purity of the phosphor. The refinement procedure involves fine-tuning various parameters of the mathematical model to accomplish the best fit between the experimental and calculated diffraction patterns. The Rietveld refinement was executed proficiently for the given phosphor with $\chi^2 = 1.5095$ and it is depicted in Fig. 5(b). The quantification analysis has shown that $99.75 \pm 0.02\%$ of CMW is present in the prepared sample, signifying that the sample is predominantly composed of CMW. Also, It was found that the given phosphor has a monoclinic structure with a space group of P 21/n. Table 1 and Table 2 summarize the structural parameters, including atomic positions, lattice parameters, and other key structural details. These findings align well with the previously reported values. Finally, we have constructed the unit cell of CMW based on the refined data, as illustrated in Fig. 5(c). This visual representation of the CMW phosphor's structure serves as a valuable tool for facilitating further analysis and result interpretation.

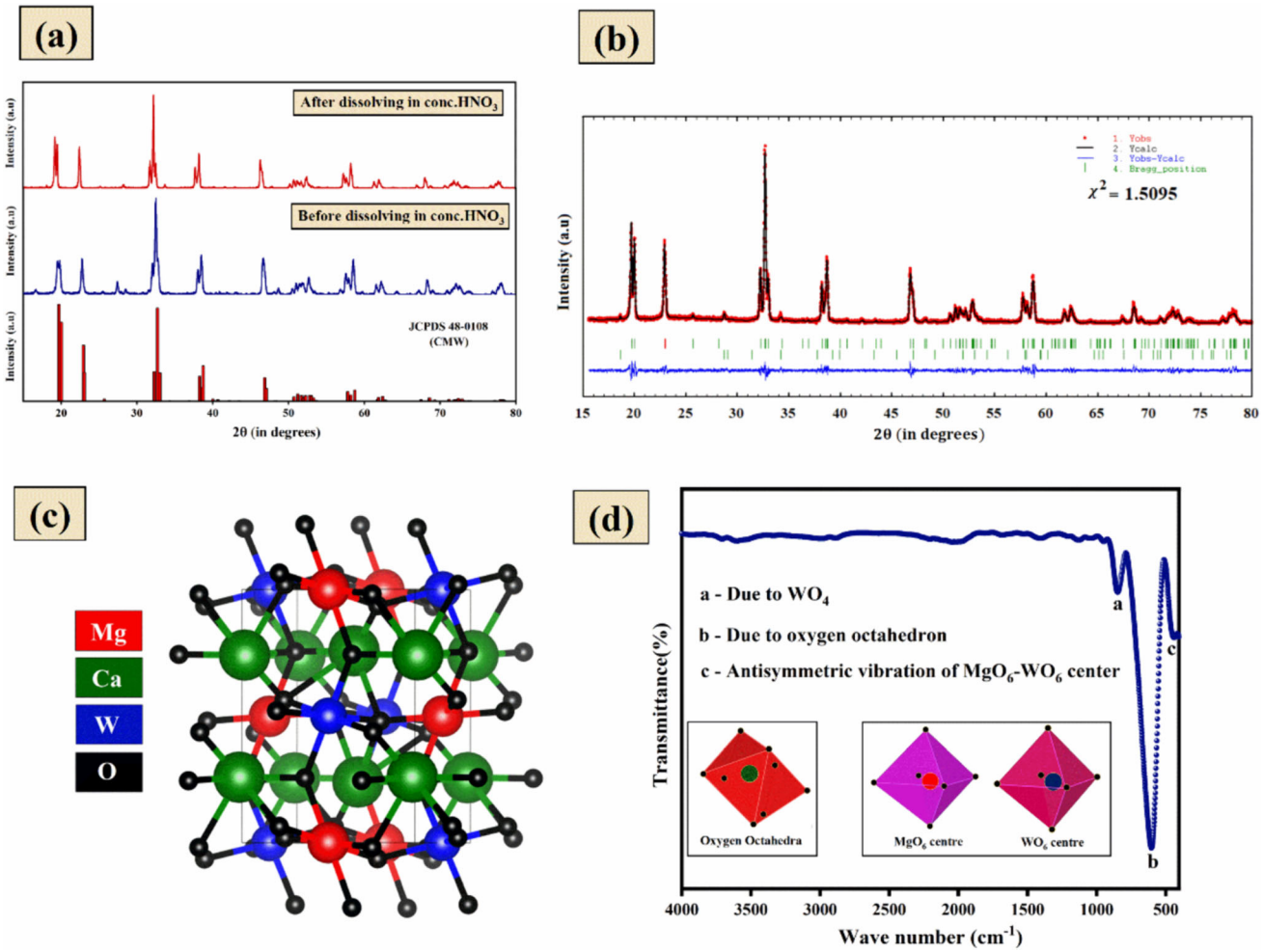

Fig. 5 (a) XRD patterns of CMW phosphor with 3% MgF_2 before and after conc. HNO_3 dissolution (b) Refinement of the pure phosphor (c) Pictorial representation of the unit cell (d) FTIR spectra of the pure CMW phosphor

Table 1 Refined structural parameters of CMW phosphor

a (Å)	b (Å)	c (Å)	V $(Å)^3$	α (°)	β (°)	γ (°)
5.41335	5.54041	7.70788	231.17611	90.00000	90.07422	90.00000

Table 2 Atomic positions of elements in CMW phosphor

	Ca	Mg	W	O1	O2	O3
x	0.01738	0.00000	0.50000	0.18892	− 0.28750	0.39939
y	0.04472	0.50000	0.00000	0.80846	0.69874	0.01678
z	0.24694	0.00000	0.00000	0.03861	− 1.05408	-0.23994

Proceeding further, we have presented the Fourier Transform Infrared (FTIR) spectrum of the prepared sample in Fig. 5(d). It is evident that there are distinct peaks present at 400 cm^{-1}, 600 cm^{-1}, and 800 cm^{-1} respectively. These peaks are ascribed to the antisymmetric vibration of MgO_6–WO_6, the breathing vibration of the oxygen octahedron, and the vibration of WO_4 respectively [28]. Furthermore, additional peaks are perceivable at 3300–3500 cm^{-1} and 1500 cm^{-1} which may be attributed to the O–H bond, likely originating from the moisture content of the sample [29].

Morphological studies of the prepared phosphor were carried out using Scanning Electron Microscopy (SEM) and the SEM image along with EDS mapping is presented in Fig. 6(a) and (b) respectively. Here we can observe that the particles are irregular and their size ranges from 1 to 4 μm. The erratic shapes of the particles are due to the inherent morphological feature of samples produced via the high-temperature solid-state method [30]. EDS mapping indicates that the sample contains Ca, Mg, W, and O elements and exhibits the average composition of W/Mg/Ca = 1:1.2:2.2, which is close to the theoretical ratio of W/Mg/Ca = 1:1:2. Next, we focus on evaluating the optical properties of the phosphor. To determine the phosphor's optical band gap, we rely on data obtained from Diffuse Reflectance Spectroscopy (DRS) [31]. We employ Tauc's equation for the band gap calculation, which is expressed as follows [32]

$$[F(R).h\nu]^{\frac{1}{m}} = B\left(h\nu - E_g\right) \quad (1)$$

where, hν = energy of the incident light in eV, B is energy independent constant, and m = 0.50 and 2 for direct band gap and indirect band gap respectively. F(R) is called as Kubelka–Munk function, and it is given by [33]

$$F(R) = \frac{K}{S} = \frac{(1-R)^2}{2R} \quad (2)$$

where R, S, and K are, reflectance, scattering coefficient, and absorption coefficient, respectively. The plot of $[F(R).h\nu]^{\frac{1}{m}}$ against hν, is a straight line with an x-intercept

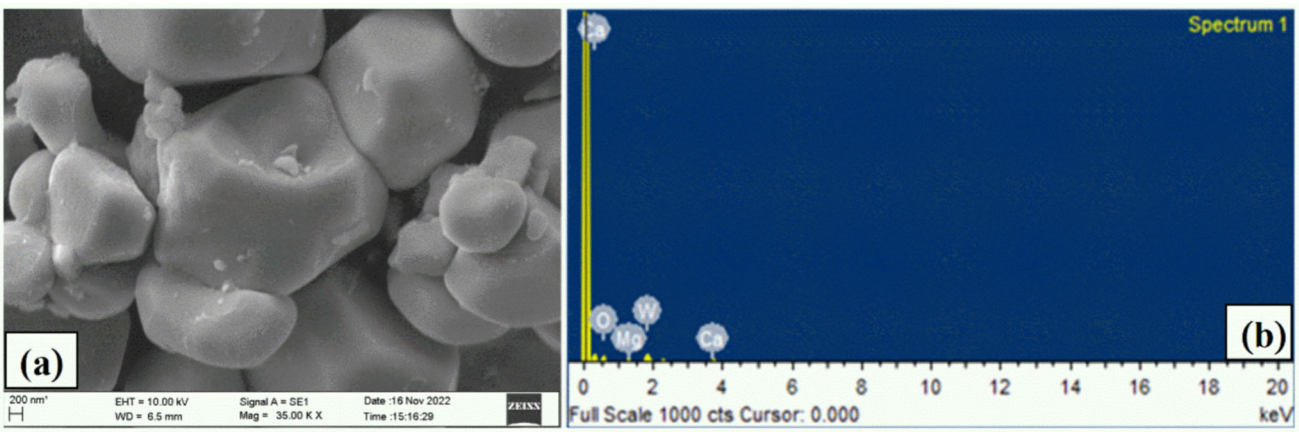

Fig. 6 (a) SEM image and (b) Elemental composition of CMW phosphor

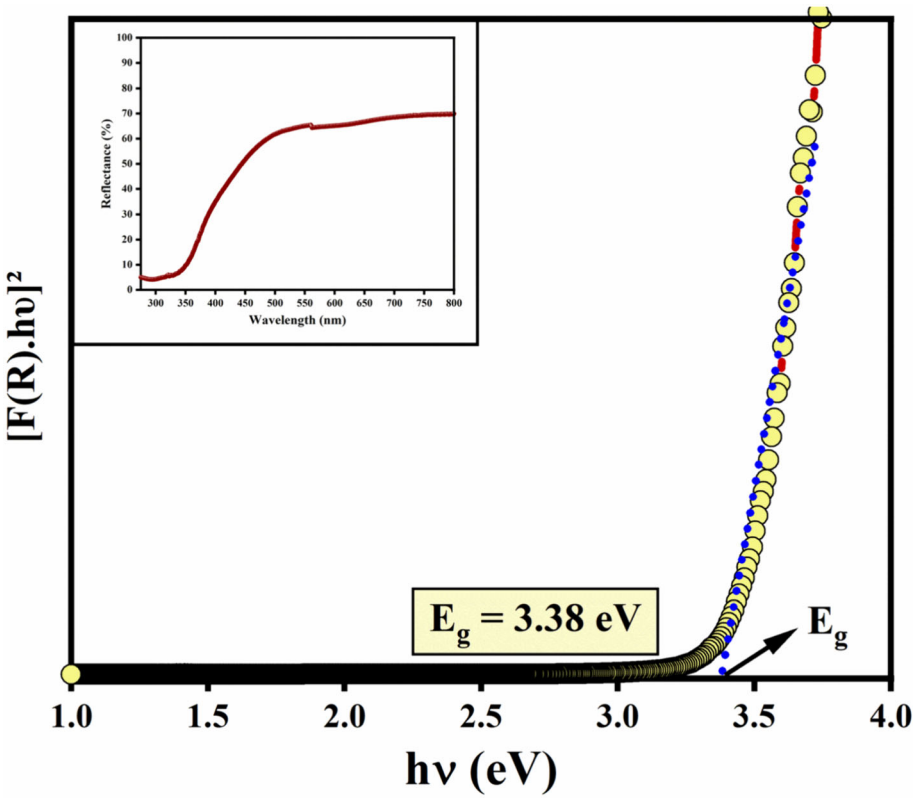

Fig. 7 Tauc's plot for the CMW phosphor and the insert shows the variation of reflectance with wavelength

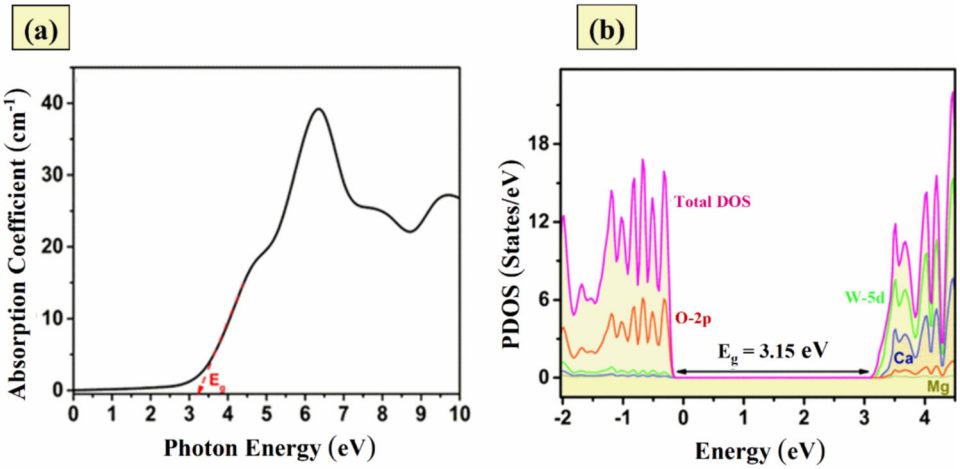

Fig. 8 (a) Simulated optical absorption spectra of CMW phosphor (b) Partial density of states of CMW phosphor

equal to the optical band gap of the material. We observed a larger R^2 value for the linear fit of $[F(R).h\nu]^{\frac{1}{m}}$ versus hν when m was set as 1/2. Hence, we determined that the phosphor possesses a direct band gap of 3.38 eV by considering the x-intercept of the linear fit as shown in Fig. 7. We have also simulated optical absorption spectra using the first principle calculation of CMW and it is found that the experimental optical bandgap is closely matched with simulated values (i.e., ∼ 3.15 eV). Figure 8(a) shows simulated optical absorption spectra. To see the electronic transition from the valance band to the conduction band a first principle approach has been utilized to estimate the density of states of CMW. Figure 8(b) shows the partial density of states of CMW phosphor for individual atoms, and it clearly shows that optical and electronic band gaps are almost similar.

Photoluminescence (PL) spectra of the CMW phosphor are shown in Fig. 9 (a). It can be seen that the PL spectrum for the phosphor with a prominent peak corresponding to blue light at 445 nm for an exciting radiation of 280 nm. The Broad PL band of CMW covers the region from 350 to

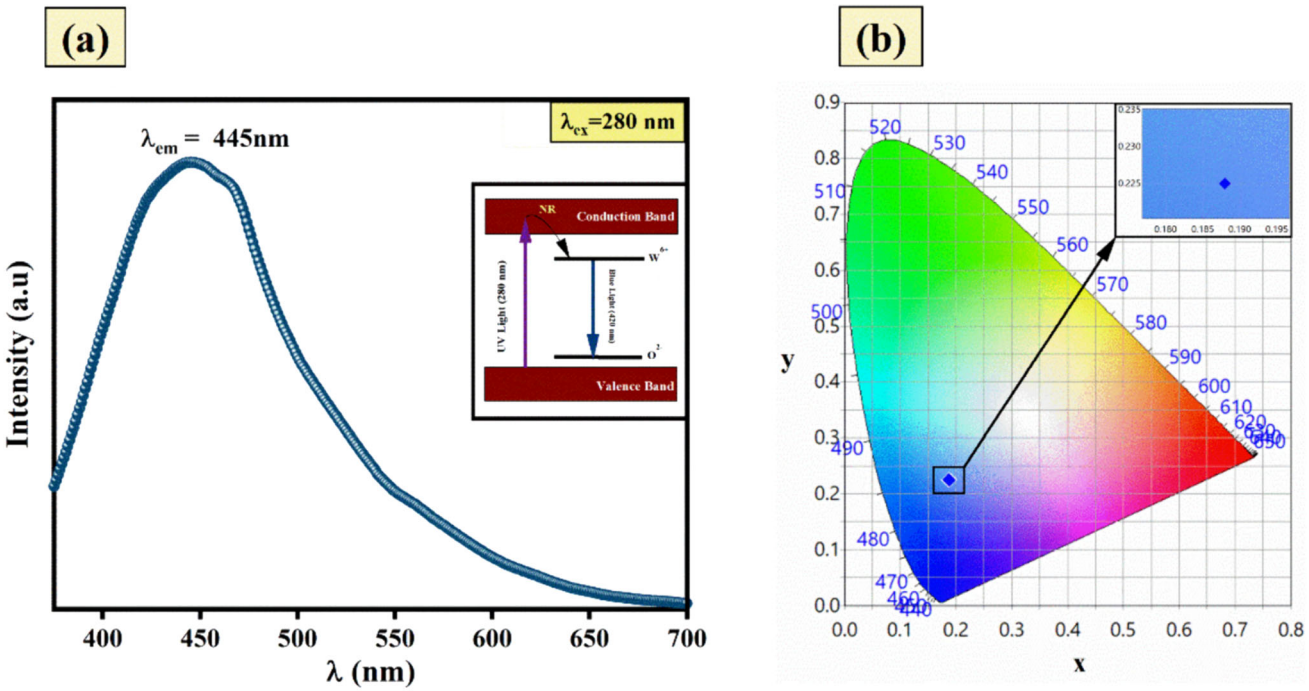

Fig. 9 (a) Emission spectrum for CMW phosphor with insert showing the emission process (b) CIE color chromaticity diagram of CMW phosphor

Fig. 10 TGA curve for CMW phosphor

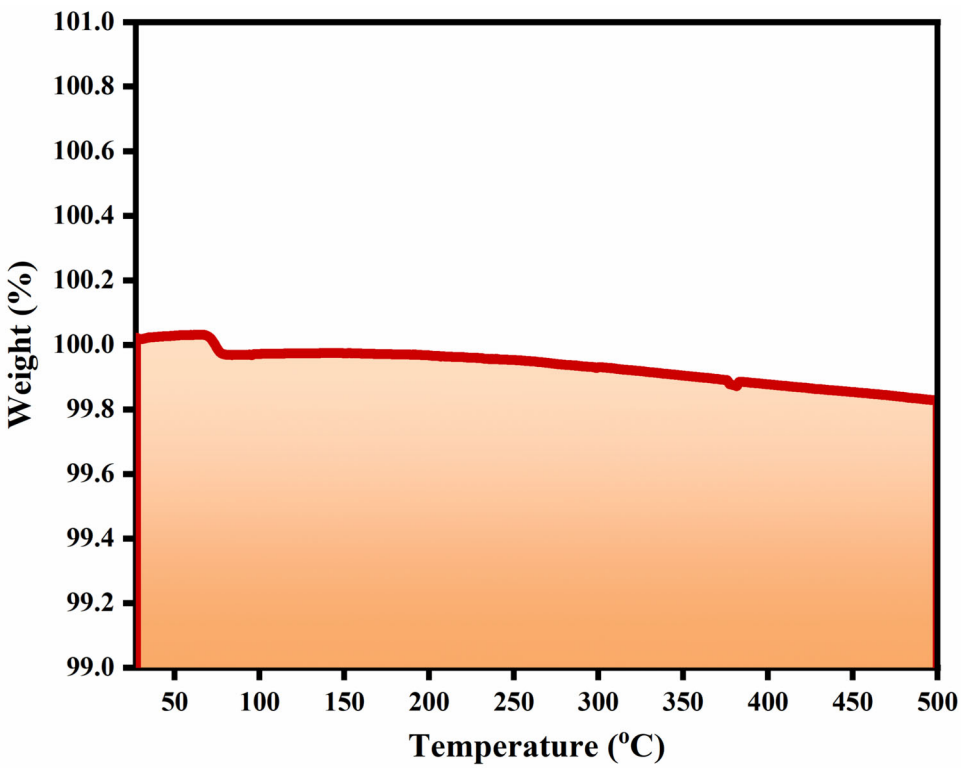

550 nm primarily attributed to the transition from W^{6+} to O^{2-} within the [WO_6] group [8, 9].

Next, we calculate CIE chromaticity coordinates using the equations [34]

$$x = \frac{X}{X + Y + Z} \tag{3}$$

$$y = \frac{Y}{X + Y + Z} \tag{4}$$

where X, Y, and Z are the tristimulus values and are given by [35]

$$X = k \int_{380\ nm}^{780\ nm} \phi(\lambda)\ \bar{x}\ (\lambda) d\lambda \tag{5}$$

$$Y = k \int_{380\ nm}^{780\ nm} \phi(\lambda)\ \bar{y}\ (\lambda) d\lambda \tag{6}$$

$$Z = k \int_{380\ nm}^{780\ nm} \phi(\lambda)\ \bar{z}\ (\lambda) d\lambda \tag{7}$$

Here k is a constant, $\phi(\lambda)$ is the color stimulus function, $\bar{x}(\lambda)$, $\bar{y}(\lambda)$, and $\bar{z}(\lambda)$ are the color-matching functions in the CIE 1931 standard observer. According to the CIE recommendation, the integration can be carried out by numerical summation at wavelength intervals $\delta\lambda$ equal to 1 nm. Hence, we get

$$X = k \sum_{380}^{780} \phi(\lambda)\ \bar{x}\ (\lambda) \delta\lambda \tag{8}$$

$$Y = k \sum_{380}^{780} \phi(\lambda)\ \bar{y}\ (\lambda) \delta\lambda \tag{9}$$

$$Z = k \sum_{380}^{780} \phi(\lambda)\ \bar{z}\ (\lambda) \delta\lambda \tag{10}$$

Using the above-mentioned equations, calculated CIE 1931 coordinates are $(0.188, 0.225)$ and it is shown in Fig. 9 (b).

At last, we inspect the thermal stability, decomposition pathways, and the presence of impurities in the phosphor using the Thermogravimetric Analysis (TGA) curve for a heating rate of 5 °C/min. The TGA curve is displayed in Fig. 10, and it can be inferred that the CMW phosphor is resilient to thermal degradation since nearly 99.85% of the sample remains unaltered within the temperature range of 30–500 °C. The loss of mass observed is predominantly attributed to the moisture content present in it [36].

Conclusions

In the present work, we have dealt with a frequently encountered obstacle in the creation of phosphor materials, which is the formation of impure phases. Although the base matrix for assorted phosphors may differ from one application to another, the approaches required to eliminate the impurity remain the same. As an illustrative case, we have selected Ca_2MgWO_6 (CMW) and successfully removed the impurities resulting from the reduction in MgO mass. It was deduced that amidst the various methods evaluated, flux-assisted synthesis was found to be adequate for the production of phosphor with 3 wt% MgF_2 as the optimum flux concentration. After the synthesis, we perform various characterizations and evaluate its fundamental characteristics. Rietveld refinement revealed that the phosphor was found to be nearly 99.75 ± 0.02% pure with particle sizes ranging from 1 to 4 μm. The optical properties of the phosphor were found to indicate an indirect band gap with a value of 3.38 eV. This agreed with the experimental optical bandgap which was simulated using first principle calculation. Also, the partial density of states of CMW shows that the optical and electronic band gaps are almost similar. Additionally, the phosphor exhibited the emission in the blue region for NUV excitation and also it was found to be thermally stable up to 500 °C. Furthermore, a comprehensive investigation can be undertaken to evaluate the suitability of flux-assisted synthesis in the production of various pristine and doped tungstate phosphor systems devoid of impurities. Additionally, a comparative analysis of the intrinsic properties of phosphors synthesized via flux-assisted methods versus those prepared using alternative techniques can be conducted to ascertain the optimal synthesis method for doped phosphors. This detailed study would provide valuable insights into the suitability and impact of flux on the quality and performance of the resulting phosphors.

References

[1] V B Pawade and S J Dhoble *Phosphors for energy saving and conversion technology*, vol 1 (Florida: CRC Press) p 83 (2018)
[2] W M Yen, S Shionoya and H Yamamoto *Practical applications of phosphors*, vol 2 (Florida: CRC Press) p 111 (2018)
[3] X Zhang et al *Journal of the American Ceramic Society***97** 246 (2014).
[4] L Gan, Z Y Mao, Y Q Zhang, F F Xu, Y C Zhu and X J Liu *Ceramics International***39** 4633 (2013).
[5] J H Bode and A B Van Oosterhout *Journal of Luminescence***10** 237 (1975).
[6] J C da Silva Oliveira, R A Ferreira and Y P Yadava *Materials Science Forum***727** 731 (2012).

[7] S J Patwe, S N Achary, M D Mathews and A K Tyagi *Materials chemistry and physics***98** 486 (2006).
[8] R Cao, G Quan, Z Shi, Z Luo, Q Hu and S Guo *Journal of Luminescence***181** 332 (2017).
[9] D Xu, X Wu, Q Zhang, W Li, T Wang, L Cao and J Meng *Journal of Alloys and Compounds***731** 156 (2018).
[10] R Cao, H Xu, W Luo, Z Luo, S Guo, F Xiao and H Ao *Materials Research Bulletin***81** 27 (2016).
[11] V Anselm and T Jüstel *Inorganics***9** 23 (2021).
[12] D Xu, Q Zhang, X Wu, W Li and J Meng *Materials Research Bulletin***110** 135 (2019).
[13] T H Q Vu, D Stefańska and P J Dereń *Inorg Chem***62** 20020 (2023).
[14] D Stefańska, B Bondzior, M Winiarski and P J Dereń *Ceram Int***49** 16038 (2023).
[15] T H Q Vu, B Bondzior, D Stefańska and P J Dereń *Dalton Transactions***51** 8056 (2022).
[16] T H Q Vu, B Bondzior, D Stefańska and P J Dereń *J Lumin***257** 119750 (2023).
[17] A W Du, Z H Zhang, S R Zhang, P H He, X M Wang and H Jiao *Materials Today Chemistry***34** 101827 (2023).
[18] B Han, J Zhang, P Huang, J X Yu and L Zhao *Journal of Optoelectronics and Advanced Materials***20** 74 (2018).
[19] J Xie and X Zhang *IOP Conf Ser Earth Environ Sci***639** 012030 (2021).
[20] L J Li, J Y Chen, Y C Jiang, S J Xu and H Guo *J Lumin***258** 119782 (2023).
[21] D Stefańska, B Bondzior, T H Vu, N Miniajluk-Gaweł and P J Dereń *Journal of Alloys and Compounds***842** 155742 (2020).
[22] P Gallagher and D W Johnson Jr *Thermochimica Acta***6** 67 (1973).
[23] H K Chen et al *IOP Conf Ser: Mater Sci Eng***170** 012035 (2017).
[24] P Giannozzi et al *Journal of Physics: Condensed matter***29** 465901 (2017).
[25] P Singh et al *Journal of Alloys and Compounds.***889** 161663 (2021).
[26] N Saadatkhah, G A Carillo, S Ackermann, P Leclerc, M Latifi, S Samih, G S Patience and J Chaouki *The Canadian Journal of Chemical Engineering***98** 34 (2020).
[27] K Vlášková, R H Colman and M Klicpera *Materials Chemistry and Physics***258** 123868 (2021).
[28] Y Wang, J Lv, J Wang, F Shi and Z M Qi *Ceramics International***47** 17784 (2021).
[29] P Gupta, A C Dillon, A S Bracker and S M George *Surface science***245** 360 (1991).
[30] N Miniajluk, B Bondzior, D Stefańska and P J Dereń *Journal of Alloys and Compounds***802** 190 (2019).
[31] G Kortüm, W Braun and G Herzog *Angewandte Chemie International Edition***2** 333 (1963).
[32] C Malik, R K Meena, P Rathi and B Singh *A Pandey Radiation Physics and Chemistry***168** 108561 (2020).
[33] P Makuła, M Pacia and W Macyk *The journal of physical chemistry letters***9** 6814 (2018).
[34] R J Mortimer and S V Thomas *Displays***32** 35 (2011).
[35] W B Cowan *Computer Graphics***17** 315 (1983).
[36] R Artiaga, S Naya, A Garcia, F Barbadillo and L García *Thermochimica acta***428** 137 (2005).